

Actinide–Silicon Multiradical Bonding: Infrared Spectra and Electronic Structures of the $\text{Si}(\mu\text{-X})\text{AnF}_3$ ($\text{An} = \text{Th}, \text{U}; \text{X} = \text{H}, \text{F}$) Molecules

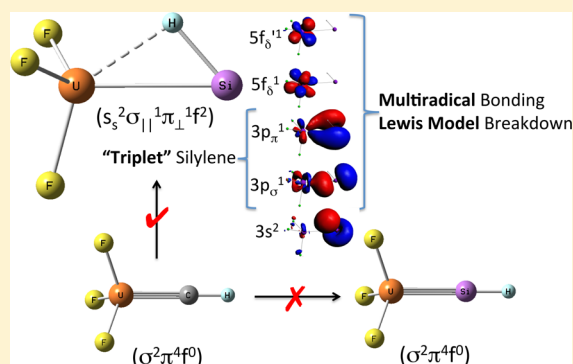
Han-Shi Hu,[†] Fan Wei,[†] Xuefeng Wang,[‡] Lester Andrews,^{*,‡} and Jun Li^{*,†}

[†]Department of Chemistry and Key Laboratory of Organic Optoelectronics and Molecular Engineering of Ministry of Education, Tsinghua University, Beijing 100084, China

[‡]Department of Chemistry, University of Virginia, Charlottesville, Virginia 22904-4319, United States

S Supporting Information

ABSTRACT: We report a series of $\text{Si}(\mu\text{-X})\text{AnF}_3$ ($\text{An} = \text{Th}, \text{U}; \text{X} = \text{H}, \text{F}$) complexes with silicon–actinide(IV) single bonds and unexpected multiradical features that form rare triplet silylenes. These bridged molecules have been prepared in microscopic scale through reactions of laser-ablated uranium and thorium atoms with silicon fluorides and identified from infrared spectra in argon and neon matrixes and relativistic quantum chemical calculations. Similar neon matrix experiments for the reactions of uranium with CF_4 and CHF_3 were carried out for comparison. Our density functional theory calculations show that the $\text{Si}\text{-U}$ single-bonded species $\text{Si}(\mu\text{-X})\text{UF}_3$ ($\text{X} = \text{H}, \text{F}$) with U(IV) oxidation state and the quasi-agostic bridge ligand of H or F are most stable among all the isomers, whereas the naively anticipated triple-bonded species $\text{XSi}\equiv\text{UF}_3$ with U(VI) oxidation state and the double-bonded species $\text{XSi}^{\bullet}=\bullet\text{UF}_3$ with U(V) oxidation state lie markedly higher in energy. Similar thorium products from reactions with XSiF_3 are also found to prefer the $\text{Si}(\mu\text{-X})\text{ThF}_3$ structures with $\text{Si}\text{-Th}$ single bonds and bridged H or F ligands. High level *ab initio* wave function theory calculations with the CCSD(T) and CASPT2 methods confirm that the ground states are quintet for $\text{Si}(\mu\text{-X})\text{UF}_3$ and triplet for $\text{Si}(\mu\text{-X})\text{ThF}_3$ with two unpaired electrons on the silylene group. These silicon-bearing molecules as the lowest-energy isomer of XSiAnF_3 represent the first silicon–actinide systems with unusual “triplet” silylenes and $\text{Si}\text{-An}$ single bonds with multiradical character. They are in dramatic contrast to the uranium–carbon analogs, $\text{XC}\equiv\text{UF}_3$, which form triple-bonded singlet ground states with C_{3v} symmetry. The calculated vibrational frequencies of the $\text{Si}(\mu\text{-X})\text{AnF}_3$ complexes agree well with experimental observations. These results accentuate the critical difference of chemical bonding of 3p- and 2p-row main-group elements with actinides. The Lewis electron-pair model and the octet rule break down for these silicon compounds.



INTRODUCTION

A large number of inorganic complexes with multiple bonds are known for main-group and transition-metal elements.^{1–4} Multiple bonding involving actinides is less common but often exhibits novel features as exemplified by the quintuple bonds of the U_2 molecule.⁵ Chemical compounds with multiple-bonds between actinides (An) and main group elements (E) have taken on considerable recent interest^{6–14} due to their potential applications in synthesis and catalysis.^{15,16} Uranium is one of the most popular paradigms, which forms numerous $\text{U}=\text{O}$ bonds, but only a few $\text{U}=\text{NR}$ and $\text{U}=\text{CR}_2$ bonds are known.¹⁷ Imido ($\text{An}=\text{NR}$), phosphinidene ($\text{An}=\text{PR}$) and $\text{N}\text{-U}\text{-N}$ linkages^{7,18,19} and $\text{U}\equiv\text{N}$ containing compounds have been synthesized.^{20–22}

Reactions of laser-ablated uranium atoms with halomethanes have been productive owing to the favorable energy or thermodynamics for the formation of new $\text{An}\text{-X}$ bonds ($\text{An} = \text{actinides}$, $\text{X} = \text{halogen}$). This pathway has led to the

successful preparation of a number of complexes with An multiple bonds. A series of double-bonded $\text{HN}=\text{UH}_2$, $\text{H}_2\text{C}=\text{UHX}$, and $\text{H}_2\text{C}=\text{UX}_2$ molecules ($\text{X} = \text{H}, \text{F}$),^{23–27} triple-bonded $\text{HC}\equiv\text{UF}_3$ and $\text{FC}\equiv\text{UF}_3$ molecules,²⁸ and quadruple-bonded $\text{C}\text{-UO}$ molecule^{29,30} were prepared in matrix isolation experiments and characterized using infrared spectroscopy and quantum chemistry methods. The same approach has been extended to the $\text{N}\equiv\text{UF}_3$, $\text{P}\equiv\text{UF}_3$, and $\text{As}\equiv\text{UF}_3$ molecules, and through CASPT2 (complete active space with second-order perturbation theory) calculations a stronger triple bond was found for nitrogen than for phosphorus and arsenic.³¹

As being congener to carbon element, silicon also has rich chemistry in synthetic chemistry and materials science, even though few actinide–silicon compounds have been synthesized.^{32,33} The preparation of molecules with $\text{C}\equiv\text{U}$, $\text{P}\equiv\text{U}$, and

Received: September 18, 2013

Published: January 2, 2014

As≡U bonds raises the question whether Si–U multiple bonds are feasible. The uranium(IV) silyl species isolated by the Cummins group is the only compound with an experimentally characterized Si–U single bond.^{34,35} So far no silicon–actinide multiple-bonded complexes are known. In comparison, while homoatomic multiple-bonded compounds for carbon such as alkenes and alkynes are rather common, the analogous disilenes, disilynes, and Si≡C-bearing compounds were more challenging to prepare^{36–39} due to lack of effective 3s–3p hybridization.⁴⁰

To investigate whether small molecules containing Si–An multiple bonds are stable and whether classic Lewis electron pair model or octet rule still can be used to predict the electronic structures of actinides with heavy main-group elements (e.g., Si), we designed a strategy to search for multiple-bonded actinide–silicon species such as XSi≡UF₃ or XSi≡ThF₃, where Si≡Th represents a doubly occupied σ -bonding orbital and two one-electron π -bonding orbitals between Si and Th. Theoretical calculations are used to determine the geometries, ground states, and spectroscopic assignments. Such theoretical investigations also help to elucidate the bonding nature of Si–An linkages and to compare the bond orders between Si–An and C–An bonds. To our surprise, instead of forming the triple-bonded linear XSi≡UF₃ singlet complexes akin to the carbon analogues with C_{3v} symmetry, we found that quintet states of Si(μ -X)UF₃ complexes with unusual quasi-agostic bridges are formed. In these complexes, the Si–An bonding involves two one-electron bonds, and Si does not fulfill the octet valence shell, leading to a breaking down of the Lewis electron-pair model.

A parallel investigation of thorium–silicon species has been performed for comparison. It is shown that Th also forms the quasi-agostic bridged Si(μ -X)ThF₃ species with triplet ground states and Si–Th single bonds. Here the Si(μ -X)ThF₃ complex is energetically more stable than the electron-deficient nonbridged XSi≡ThF₃ (C_{3v}) molecule, where a complete triple-bond could not be formed due to the limit of the four valence electrons for thorium. In contrast, the carbon analogues favor the XC≡ThF₃ (C_{3v}) structure, as observed previously.^{41,42}

EXPERIMENTAL AND THEORETICAL METHODS

Uranium atoms were produced by laser ablation of a depleted square metal piece obtained from Oak Ridge National Laboratory (ORNL) using methods described previously^{25–29,32,42,43,43,44} and codeposited with silicon fluoride samples diluted by argon (0.5%) or neon (0.3%) onto a 4 K infrared transmitting substrate. The SiF₄ (Matheson) sample was condensed at 77 K and outgassed to remove any volatile impurities. Silicon hydrogen fluorides, SiHF₃ (synthesized by Willner using AsF₃ and SiHCl₃) or SiDF₃ (synthesized by Willner from the reaction of DCl and Si to form SiDCl₃, followed by fluorination using SbF₃ as described by Burger and co-workers),⁴⁵ were treated in like fashion. Similar experiments were performed using thorium metal from ORNL. Infrared spectra were recorded on a Nicolet 750 spectrometer after sample deposition, after annealing, and after irradiation using a 175 W mercury arc street lamp with the globe removed. Additional neon matrix experiments were also performed for the reactions of uranium with CF₄ and CHF₃ for comparison to the earlier argon matrix spectra²⁹ and to the present neon matrix observations of the silicon species.

The geometries, electronic structures, and vibrational frequencies of the uranium and thorium reaction products were calculated using relativistic density functional theory (DFT) and wave function theory (WFT). In the DFT calculations the generalized gradient approach was used with PBE exchange–correlation functional⁴⁶ as implemented in Amsterdam Density Functional (ADF 2008.01) program.^{47–49} In

these calculations we used the zero-order regular approximation (ZORA)⁵⁰ for the scalar relativistic effects and uncontracted Slater basis sets with triple- ζ plus two polarization functions (TZ2P).⁵¹ The frozen core approximation was applied to the [1s²] cores of C and F and [1s²–5d¹⁰] core of Th and U. The rest of the electrons were explicitly treated variationally.

The hybrid B3LYP density functional in the Gaussian 03 program was also employed for the molecules of the reaction products to compare with similar calculations for the carbon species.^{52–54} The 6-311++G(3df,3pd) basis sets for F and Si and 6-311++G(2d, p) basis set for hydrogen were used,⁵⁵ and SDD pseudopotential and basis set with 30 or 32 valence electrons were used for thorium and uranium (Basis-I hereafter),⁵⁶ where the scalar relativistic effects were included through the pseudopotentials. The vibrational frequencies were computed analytically, and zero point energy (ZPE) corrections were included in the calculations of relative energies of the products.

To verify the DFT results, we also performed single-point energy calculations using coupled-cluster with single and double and perturbative triple excitations (CCSD(T)) method⁵⁷ with the cc-pVDZ basis sets for Si and F,⁵⁸ aug-cc-pVTZ for H,⁵⁹ SDD pseudopotential (ECP60MWB), and ANO basis set for U and Th (Basis-II).⁶⁰ These CCSD(T) calculations were performed at the geometries optimized using DFT methods to help to identify the ground states for the two U + SiXF₃ and Th + SiXF₃ systems, respectively. In order to investigate any possible multiconfiguration features of these Si–U systems, geometries were further optimized using complete-active-space self-consistent field (CASSCF)⁶¹ and CASPT2 methods⁶² with the same ECPs and basis sets as above. In the CASSCF calculations for the U + SiXF₃ systems, we used an active space of 6 electrons in 11 active orbitals consisting of 3 frontier MOs of (σ)²($\sigma_{||}$)¹(π_{\perp})¹ mainly from Si 3s3p σ 3p π and 8 MOs from U 5f⁷7s⁰ orbitals, denoted as (6e,11o) hereafter, to allow for configuration mixing through nondynamic electron correlation. A CASSCF calculation with (6e, 16o) that includes U 6d orbitals shows that the occupation numbers of the 6d-based natural orbitals are <0.03, indicating that the (6e, 11o) active space is appropriate. For the Th + SiXF₃ systems a similar active space of (4e, 11o) was used, where Th(IV) 5f⁰ has two fewer electrons. The CASPT2 energy calculations and geometry optimizations were carried out to provide more reliable total energies in case of significant multireference characteristics. In the CASPT2 calculations, we selected all of the virtual orbitals and the occupied valence orbitals plus U 6s6p for the correlation. All these *ab initio* WFT calculations were carried out using MOLPRO 2008.1.⁶³

RESULTS AND DISCUSSION

We will start with presenting the infrared spectra for uranium and thorium reaction products with silicon fluorides. Figures 1–5 show the experimentally observed infrared spectra of the U + SiF₄, Th + SiF₄, U + SiHF₃, U + SiDF₃, and Th + SiHF₃ systems, respectively.

An + SiF₄. Infrared spectra for uranium reaction products with silicon tetrafluoride are compared in solid argon and neon in Figure 1. The initial argon sample deposit, which freezes faster than neon at 4 K, revealed bands at 855 and 843 cm⁻¹ for the SiF₂ intermediate, 831 and 954 cm⁻¹ for the SiF₃ radical,⁶⁴ and weak bands in this region that are also common to SiF₄ experiments using different metals (not shown). Of more interest are bands that are unique from reactions with a particular metal. With uranium, weak, new broad bands were observed at 578 and 537 cm⁻¹, which sharpened slightly on annealing to 20 K. Sequential ultraviolet irradiation increased the latter bands (Figure 1). Annealing to 30 K sharpened these features to 576.4 and 537.2 cm⁻¹. Notice that the lower band is not split and approximately triple the intensity of the higher frequency band. In solid neon the SiF₃ bands shifted to 959 and 835 cm⁻¹ and the SiF₂ bands to 864 and 851 cm⁻¹, and stronger initial product bands were observed at 587 and 549

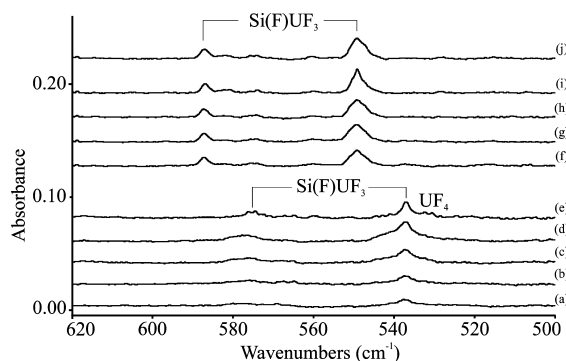


Figure 1. Infrared spectra of the major product of the U atom and SiF_4 reaction in solid argon (a–e) and neon (f–j) at 5 K. Spectrum after (a) codeposition of laser-ablated U and SiF_4 (0.5%) in argon for 60 min, (b) irradiation >320 nm for 20 min, (c) 240–380 nm irradiation, (d) >220 nm irradiation, and (e) annealing to 30 K. Spectrum after (f) codeposition of laser-ablated U and SiF_4 (0.3%) in neon for 60 min, (g) irradiation >380 nm for 20 min, (h) >290 nm irradiation, (i) 240–380 nm irradiation, and (j) annealing to 10 K.

cm^{-1} , but less growth was produced by irradiation. Annealing to 10 K sharpened the bands to 586.9 and 549.0 cm^{-1} . Again, the lower frequency band is sharp and about triple the intensity of the higher bands.

Spectra from the analogous experiments with thorium are illustrated in Figure 2. Weak, broad bands were observed at

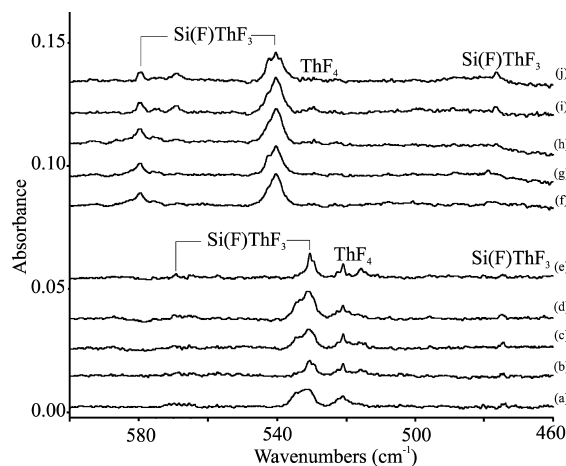


Figure 2. Infrared spectra of the major product of the Th atom and SiF_4 reaction in solid argon (a–e) and neon (f–j) at 5 K. Spectrum after (a) codeposition of laser-ablated Th and SiF_4 (0.5%) in argon for 60 min, (b) annealing to 20 K, (c) 240–380 nm irradiation for 20 min, (d) >220 nm irradiation, and (e) annealing to 30 K. Spectrum after (f) codeposition of laser-ablated Th and SiF_4 (0.3%) in neon for 60 min, (g) annealing to 8 K, (h) 240–380 nm irradiation, (i) >220 nm irradiation, and (j) annealing to 10 K.

570, 532, and 475 cm^{-1} , and the middle one is much stronger. The weak, sharp bands at 521.0 and 515.7 cm^{-1} were due to ThF_4 produced in the reaction.⁶⁵ Annealing and UV irradiation sharpened these bands to 569.3, 530.5, and 475.9 cm^{-1} . Again the product yield in the softer neon matrix is higher as the bands are observed at 579.5, 540.4, and 479.4 cm^{-1} and the final annealing favored matrix site splittings at 580.3, 542.4, and 476.8 cm^{-1} in solid neon matrix.

An + SiHF_3 . A series of similar experiments were performed with the SiHF_3 precursor. The spectra of the uranium reaction

product shown in Figure 3 appear similar to those of the An + SiF_4 systems with slightly shifted product bands. Again weak

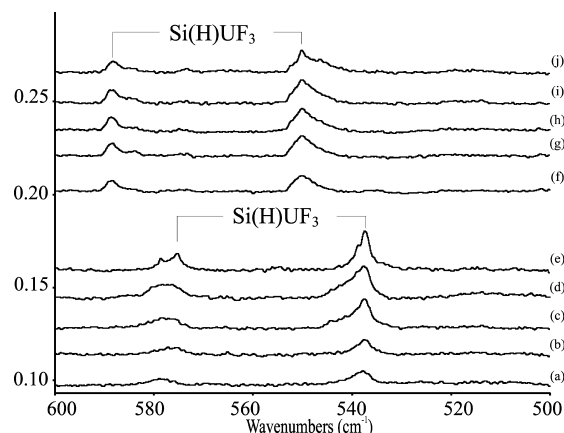


Figure 3. Infrared spectra of the major product of the U atom and SiHF_3 reaction in solid argon (a–e) and neon (f–j) at 5 K. Spectrum after (a) codeposition of laser-ablated U and SiHF_3 (0.5%) in argon for 60 min, (b) annealing to 20 K, (c) >290 nm irradiation for 20 min, (d) >220 nm irradiation, and (e) annealing to 30 K. Spectrum after (f) codeposition of laser-ablated U and SiHF_3 (0.3%) in neon for 60 min, (g) irradiation >380 nm for 20 min, (h) >290 nm irradiation, (i) >220 nm irradiation, and (j) annealing to 10 K.

broad bands were observed on sample deposition, this time at 577 and 537 cm^{-1} , which were increased 5-fold on UV irradiation and were sharpened to show peaks at 578.6, 575.3, and 537.5 cm^{-1} on annealing. A very weak broad band was observed at 1490 cm^{-1} . As before the reaction progressed further on deposition in excess neon, the final bands were observed at 588.6 and 550.1 cm^{-1} . Again, the lower band is sharp and about double the intensity of the higher frequency band.

Spectra from an experiment for uranium reacting with SiDF_3 are shown in Figure 4. The important new feature is the band at 1080 cm^{-1} , not observed with SiHF_3 precursor, which tracks on annealing and photolysis along with the 577 and 537 cm^{-1} absorptions. The latter shows no discernible deuterium shifts. This region is clean in spectra observed with the SiHF_3 precursor, which are illustrated in Figure S14 and also reveals a very weak 1051 cm^{-1} band due to NUN from reaction of U

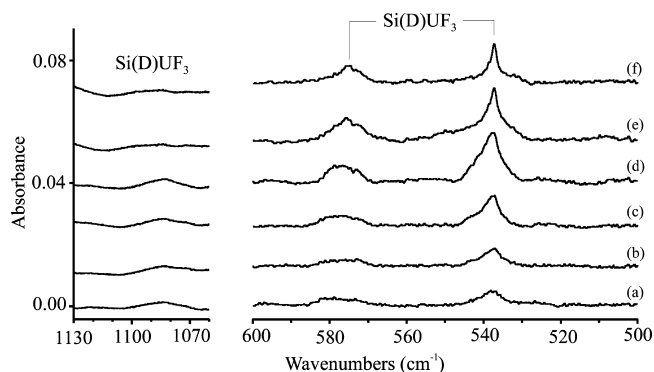


Figure 4. Infrared spectra of the major product of the U atom and SiDF_3 reaction in solid argon 5 K. Spectrum after (a) codeposition of laser-ablated U and SiDF_3 (0.5%) in argon for 60 min, (b) annealing to 20 K, (c) >290 nm irradiation, (d) >220 nm irradiation, (e) annealing to 30 K, and (f) annealing to 35 K.

with trace nitrogen impurity upon UV irradiation and the 1023 cm^{-1} absorption due to SiF_4 in the SiHF_3 sample.

The spectra for the reaction products of thorium with SiHF_3 are shown in Figure 5. Argon matrix experiments revealed

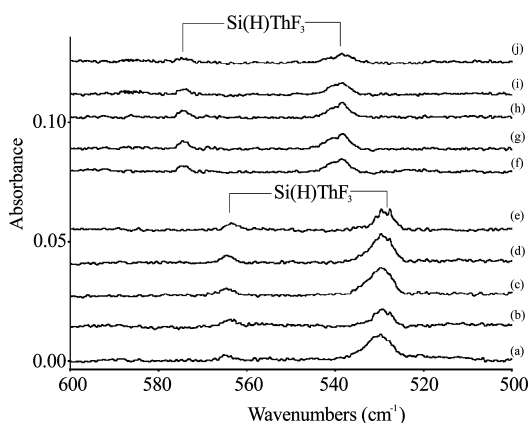


Figure 5. Infrared spectra of the major product of the Th atom and SiHF_3 reaction in solid argon (a–e) and neon (f–j) at 5 K. Spectrum after (a) codeposition of laser-ablated Th and SiHF_3 (0.5%) in argon for 60 min, (b) annealing to 20 K, (c) >290 nm irradiation, (d) 240–380 nm irradiation, and (e) annealing to 30 K. Spectrum after (f) codeposition of laser-ablated Th and SiHF_3 (0.3%) in neon for 60 min, (g) irradiation >320 nm for 20 min, (h) 240–380 nm irradiation, (i) >220 nm irradiation, and (j) spectrum after annealing to 10 K.

broad bands at 569 and 529 cm^{-1} , which increased slightly on UV irradiation and sharpened to yield peaks at 563.6, 529.6, and 527.6 cm^{-1} on annealing. In solid neon these bands shifted to 574.6, 538.5, and 536.5 cm^{-1} .

U + CF_3X . We previously reported argon matrix-isolation experiments on reactions of laser-ablated uranium with CF_3X ($\text{X} = \text{H}, \text{F}$) to form $\text{HC}\equiv\text{UF}_3$ and $\text{FC}\equiv\text{UF}_3$ molecules with C_{3v} symmetry.²⁹ In the present work, supplementary neon matrix experiments were performed for the reactions of uranium with CF_4 and CHF_3 . When comparing the peaks observed in the solid argon matrix, similar absorptions were observed in solid neon matrix: the absorptions of the $\text{FC}\equiv\text{UF}_3$ product shift to 586.6 and 545.9 cm^{-1} , and those of the $\text{HC}\equiv\text{UF}_3$ product shift to 583.9 and 549.7 cm^{-1} . This represents blue shifts of 7.9 and 9.4 cm^{-1} for the former and 7.7 and 9.5 cm^{-1} for the latter molecule upon matrix change from argon to neon, which are reasonable for these molecules.⁶⁶ Unlike in other actinide molecules (e.g., CUO and UO_2) that prefer different ground states in neon and argon matrices,^{67–70} the present results attest that the same ground states of the $\text{XC}\equiv\text{UF}_3$ ($\text{X} = \text{H}, \text{F}$) molecules are trapped for both uranium methylidyne molecules in solid neon as in argon.²⁹

Identifying the Reaction Products of the U + SiXF_3 System. At a first glance the infrared spectra for the U and SiF_4 reaction product are similar to the spectra observed for the U and CF_4 reaction product, but there are markedly identifiable differences.²⁹ The silicon product bands are slightly stronger and about double the bandwidth, and the higher frequency band is 2 cm^{-1} higher, and the lower band is 1 cm^{-1} lower. Both are characteristic spectra for the symmetric and antisymmetric U–F stretching vibrations, expected for a UF_3 group. Importantly, the U–F vibrations of $\text{N}\equiv\text{UF}_3$ are in the same region.³²

To help to identify the products and characterize the bonding characteristics and electronic states of these Si–U

systems, we have performed systematic geometry optimizations using DFT methods on all possible products from reactions of $\text{U} + \text{SiXF}_3$ ($\text{X} = \text{H}, \text{F}$). The calculations are carried out for several spin multiplicities of all the isomers A, B, C, and D shown in Scheme 1.

Scheme 1. An Illustration of the Reaction Products of Uranium and SiXF_3 ($\text{X} = \text{H}, \text{F}$)

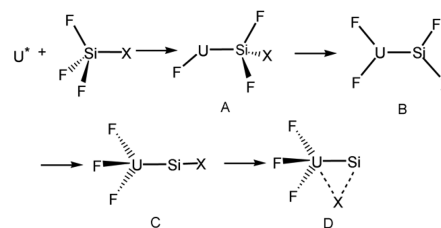


Table 1 lists the relative energies of the possible products (A, B, C, and D with different spin-multiplicities) of the $\text{U} + \text{SiXF}_3$

Table 1. Relative DFT and CCSD(T) Energies for XSUUF_3 ($\text{X} = \text{H}, \text{F}$) Isomers Calculated at the Optimized PBE Geometries^{a,b}

isomer		X = H		X = F	
		ΔE_{PBE}	$\Delta E_{\text{CCSD(T)}}$	ΔE_{PBE}	$\Delta E_{\text{CCSD(T)}}$
A	$\text{F}_2\text{XSU}-\text{UF}$	33.18	–	29.92	–
B	$\text{FXSU}-\text{UF}_2$	8.40	–	9.52	–
C_S	$\text{XSU}\equiv\text{UF}_3$	6.93	14.17	12.25	17.73 ($\sigma^2\pi^4f^0$)
C_T	$\text{XSU}^*\equiv\text{UF}_3$	4.79	/	9.47	18.60 ($\sigma^2\pi^3f^1$)
C_Q	$\text{XSU}\div\text{UF}_3$ ^d	2.16	3.70	7.61	13.92 ($\sigma^2\pi^2f^2$)
D_T'	$\text{Si}(\mu\text{-X})-\text{UF}_3$	19.67	15.89	11.00	6.66 ($\sigma_s^2\sigma_{\parallel}^2\pi_{\perp}^0f^2$)
D_T	$\text{Si}(\mu\text{-X})-\text{UF}_3$	2.47	13.77	–2.76	4.86 ($(\sigma_s^2\sigma_{\parallel}^2\pi_{\perp}^1f^1)$)
D_Q	$\text{Si}(\mu\text{-X})-\text{UF}_3$	0.00	0.00	0.00	0.00 ($\sigma_s^2\sigma_{\parallel}^1\pi_{\perp}^1f^2$)

^aAll the energies (in kcal/mol) are relative to those of the quintet $\text{Si}(\mu\text{-X})-\text{UF}_3$ isomer. ^bThe DFT energies are obtained from PBE/TZ2P geometry optimizations with scalar relativistic ZORA Hamiltonian; the UCCSD(T) single-point energies are calculated with Basis-II. ^c C_S refers to the singlet state with $\text{Si}\equiv\text{U}$ triple bond, C_T refers to the triplet state with $\text{Si}^*\equiv\text{U}$ double bond, C_Q refers to the quintet state with $\text{Si}\div\text{U}$ double bond. D_T' , D_T , and D_Q denote, respectively, the two triplet and one quintet states with Si–U single bond (see Scheme 1 and Figure 6). ^dThere are two imaginary frequencies (93i and 75i cm^{-1}) of H–Si–U bending mode for quintet $\text{HSi}\div\text{UF}_3$, which leads to the Si–H–U bridged structure by reoptimization following the imaginary frequencies.

system from DFT PBE geometry optimizations and CCSD(T) single-point energy calculations. Figure 6 depicts the optimized structures of the possible products of the reactions $\text{U} + \text{SiXF}_3$ ($\text{X} = \text{H}, \text{F}$) calculated by using PBE/TZ2P level of theory. For the $\text{U} + \text{SiHF}_3$ system, both the optimized DFT energies and the CCSD(T) single-point energies suggest that the quintet state of the quasi-agostic $\text{Si}(\mu\text{-H})\text{UF}_3$ structure is most stable, corresponding to the structure D in Scheme 1. Interestingly, the lowest-energy quintet state has a $\sigma_s^2\sigma_{\parallel}^1\pi_{\perp}^1\delta^2$ configuration mainly from $\text{Si}(3s^23p_{\sigma}^13p_{\pi}^1)$ and $\text{U}(5f_{\delta}^15f_{\delta}^1)$, denoted as $\sigma_s^2\sigma_{\parallel}^1\pi_{\perp}^1f^2$ hereafter, indicating that the $\text{Si}(\mu\text{-H})\text{UF}_3$ species has a U(IV) oxidation state and a Si–U single bond instead of the anticipated $\text{Si}\equiv\text{U}$ ($\sigma^2\pi^4f^0$) or $\text{Si}^*\equiv\text{U}$ ($\sigma^2\pi^3f^1$) multiple bonds, where σ_s represents the valence orbital of lone pair on Si, σ_{\parallel} and π_{\perp} represent the weakly bonding orbitals formed between Si and U (though mainly contributed by Si atom), and

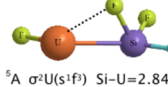
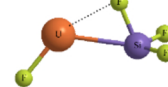
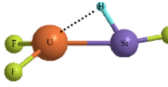
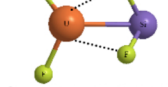
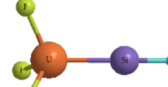
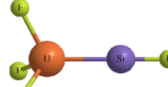
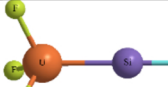
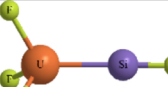
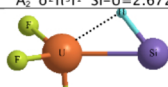
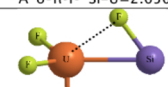
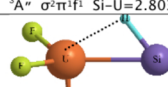
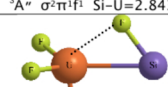
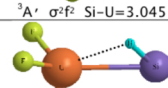
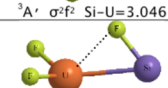
		X=H	X=F
A	$F_2XSi-UF$	 $^5A'' \sigma^2U(s^1f^1) \text{ Si-U}=2.848$	 $^5A'' \sigma^2U(s^1f^1) \text{ Si-U}=2.897$
B	$FXSi-UF_2$	 $^3A' \sigma^2\pi^2U(f^1) \text{ Si-U}=2.552$	 $^3A' \sigma^2U(f^1) \text{ Si-U}=2.758$
C ₁	$XSi-UF_3$	 $^1A_1 \sigma^2\pi^4 \text{ Si-U}=2.539$	 $^1A_1 \sigma^2\pi^4 \text{ Si-U}=2.516$
C ₂	$XSi-UF_3$	 $^3A_2 \sigma^2\pi^3f^1 \text{ Si-U}=2.672$	 $^3A \sigma^2\pi^3f^1 \text{ Si-U}=2.656$
D _T	$Si(\mu-X)-UF_3$	 $^3A'' \sigma^2\pi^1f^1 \text{ Si-U}=2.803$	 $^3A'' \sigma^2\pi^1f^1 \text{ Si-U}=2.843$
D _{T'}	$Si(\mu-X)-UF_3$	 $^3A' \sigma^2f^2 \text{ Si-U}=3.045$	 $^3A' \sigma^2f^2 \text{ Si-U}=3.046$
D _Q	$Si(\mu-X)-UF_3$	 $^5A'' s^2\sigma^1\pi^1f^2 \text{ Si-U}=2.875$	 $^5A'' s^2\sigma^1\pi^1f^2 \text{ Si-U}=2.948$

Figure 6. DFT (PBE/TZ2P) optimized structures of the possible products of the reactions of $U+SiXF_3$ ($X = H, F$). The bond lengths are in Å.

δ represents the highly localized 5f orbital on U atom. The frontier Kohn–Sham molecular orbitals (MO, σ_{Si-H} , σ_s , $\sigma_{||}$, π_{\perp} , δ , δ') of the $Si(\mu-H)UF_3$ structure are shown in Figure 7. These two singly occupied $\sigma_{||}$ and π_{\perp} bonding orbitals are mainly contributed from the nonhybridized 3p orbitals of Si element. The MO composition analysis shows that around 65% of the $\sigma_{||}$ and π_{\perp} orbitals are from the Si 3p AOs, which is further confirmed by NBO analysis as listed in Table S2. Here the SiH^- fragment in $Si(\mu-H)UF_3$ can be viewed as a deprotonated triplet silylene. The spin density contours of the triplet SiX^- and $Si(\mu-X)AnF_3$ ($X = H, F$) depicted in Figure 8 clearly show cyclic spin density distribution of two unpaired 3p-dominated $\sigma_{||}$ and π_{\perp} bonding electrons around Si atom, indicating that $Si(\mu-X)AnF_3$ is a SiX^- -bearing triplet silylene.

The calculated vibrational frequencies for the four major isomers of $XSiUF_3$ are shown in Table 2. The calculated IR frequencies and intensities of the quintet $Si(\mu-H)UF_3$ molecule agree well with the experiments. In contrast, the calculated frequencies of the multiple-bonded compounds $HSi\equiv UF_3$ and $HSi^+=UF_3$ do not agree with the observed IR spectra, consistent with their higher energies (Table 1). Unfortunately the bridged Si–H stretching modes, the fingerprints of these species, could not be observed in the experiments as they are either broadened by the matrix interaction or in the region of water absorption. On the other hand, the frequencies of the Si–

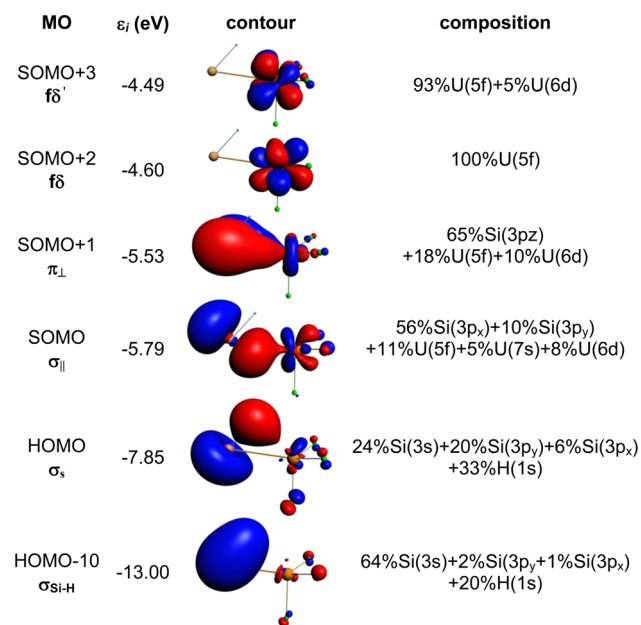


Figure 7. The isosurfaces (cutoff = 0.05 au) of the Kohn–Sham orbitals of $Si(\mu-H)UF_3$ species with a quintet ground state of $\sigma_s^2\sigma_{||}^1\pi_{\perp}^1f^2$ electron configuration.

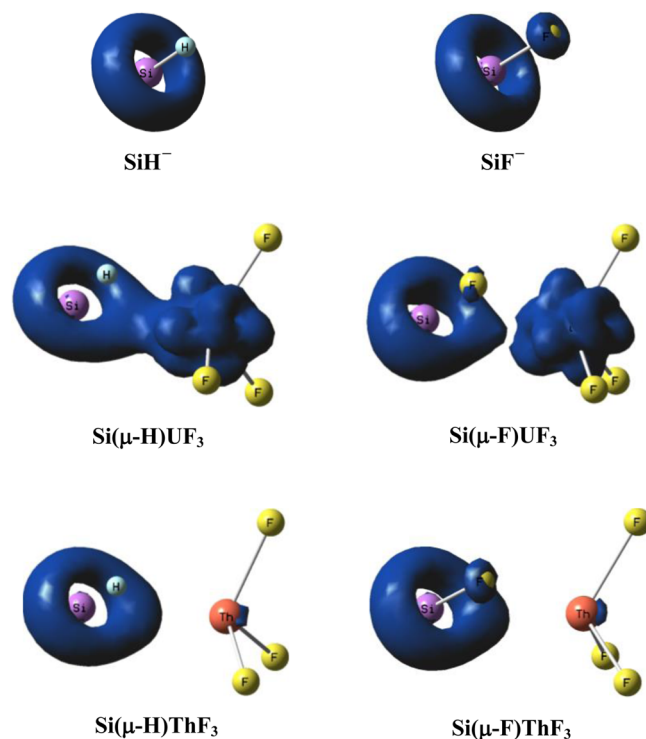


Figure 8. The spin density contour of triplet SiX^- and $Si(\mu-X)AnF_3$ ($X = H, F$; An = Th, U; quintet for $Si(\mu-X)AnF_3$ and triplet for $Si(\mu-X)AnF_3$ complex (cutoff = 0.015 au).

U stretching modes are too low to be detected in the experiments. To further verify this hydrogen-bridged Si–U molecule, we performed an experiment of $U+DSiF_3$ reaction and obtained the $Si(\mu-D)U$ stretching mode at 1080 cm^{-1} , as shown in Figure 4. This broad new feature, not observed with $SiHF_3$ precursor, tracks on annealing and photolysis with the 577 and 537 cm^{-1} absorptions. The calculated frequency of the $Si(\mu-D)U$ stretching mode of $Si(\mu-D)UF_3$ at 1151 cm^{-1}

Table 2. Observed and Calculated Vibrational Frequencies for $\text{Si}(\mu\text{-X})\text{UF}_3$, $\text{XSi}^{\bullet}=\bullet\text{UF}_3$ and $\text{XSi}\equiv\text{UF}_3$ (X = H, F) Molecules^a

mode	obs. ^b	calcd	calcd	calcd	calcd
		$\text{Si}(\mu\text{-H})\text{UF}_3(^5\text{A}')$	$\text{Si}(\mu\text{-H})\text{UF}_3(^3\text{A}')$	$\text{HSi}^{\bullet}=\bullet\text{UF}_3(^3\text{A}_1)$	$\text{HSi}\equiv\text{UF}_3(^1\text{A}_1)$
Si–H str		1601(248), 820(23)	1109(636)	2023(69)	1996(82)
U–F sy str	588.6 (Ne) 578.6 (Ar)	579(199)	555(49)	585(226)	593(202)
U–F as str	550.1 (Ne) 537.5 (Ar)	543(144), 542(145)	551(213), 501(12)	549(158)	554(297)
Si–U str					354(0.4)
		$\text{Si}(\mu\text{-F})\text{UF}_3(^5\text{A}')$	$\text{Si}(\mu\text{-F})\text{UF}_3(^3\text{A}')$	$\text{FSi}^{\bullet}=\bullet\text{UF}_3(^3\text{A}_1)$	$\text{FSi}\equiv\text{UF}_3(^1\text{A}_1)$
Si–F str		573(186)	501(49)	831(177)	836(158)
U–F sy str	586.9 (Ne)	580 (130)	578(167)	592(249)	599(227)
U–F as str	549.0 (Ne)	544(105)	548(149), 541(147)	546(290)	554(278)
Si–U str				226(1)	287(2)

^aVibrational frequencies (cm^{-1}) and intensities (km/mol , in parentheses) are calculated using DFT PBE/TZ2P (see text), with seven low-frequency bending modes omitted. ^bAbsorptions observed in neon (in bold face) and argon matrix.

compares well with the experimental one, as shown in Table S3. This experiment has provided direct evidence for the $\text{Si}(\mu\text{-D})\text{U}$ bridged structure and quasi-agostic interaction.

It is remarkable that the quintet $\text{Si}(\mu\text{-H})\text{UF}_3$ molecule is more stable than the multiple-bonded $\text{HSi}\equiv\text{UF}_3$ and $\text{HSi}^{\bullet}=\bullet\text{UF}_3$, which is in marked contrast to the $\text{U}+\text{CHF}_3$ system where singlet $\text{HC}\equiv\text{UF}_3$ with triple bonds is energetically favored.²⁹ To understand this difference we have analyzed the orbital interactions between the UF_3 fragment and SiH or CH fragments. The Kohn–Sham MO energy levels of these fragments and the $\text{HC}\equiv\text{UF}_3$ and $\text{HSi}^{\bullet}=\bullet\text{UF}_3$ molecules are shown in Figure 9. It becomes clear that $\text{HC}\equiv\text{UF}_3$ with the

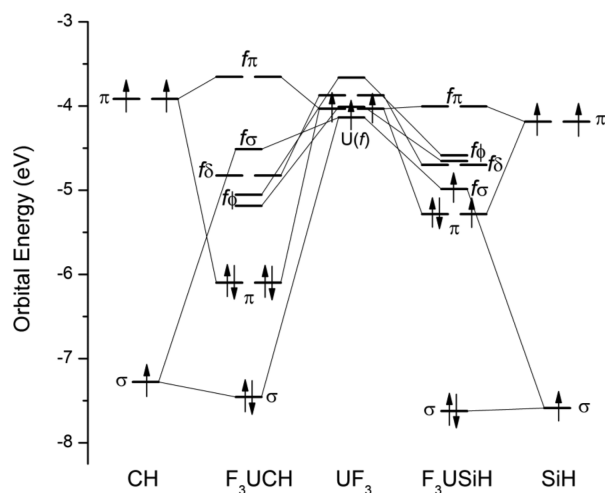


Figure 9. Comparison of orbital interactions in $\text{F}_3\text{U}\equiv\text{CH}$ and $\text{F}_3\text{U}^{\bullet}=\bullet\text{SiH}$ between the fragments UF_3 , CH , and SiH .

U(VI) oxidation state forms the $\sigma^2\pi^4f^0$ electron configuration with one σ bond and two π bonds and a large HOMO–LUMO energy gap (≈ 1 eV), where the electron configurations are shown in a local C–U linear-group notation for brevity, whereas in $\text{HSi}^{\bullet}=\bullet\text{UF}_3$ the Si–U π -bonding orbitals and the U $5f$ orbitals are rather close in energy (≈ 0.25 eV), due to the high Si $3p$ orbital energy and very small π -type orbital overlap between Si and U . As a result, multiple bonds with U(V) oxidation state can hardly be stable for the Si–U species due to dynamic Jahn–Teller instability, and it is even more difficult to form the U(VI) complex of $\text{HSi}\equiv\text{UF}_3$. Indeed, calculations on $\text{HSi}\equiv\text{UF}_3$ show that the U $5f$ orbital lies 0.1 eV below the Si–

U π -bonding orbital, implying potential spontaneous reduction of U(VI) upon formation. The optimized $\text{Si}\equiv\text{U}$ triple bond is 0.6 Å longer than the $\text{C}\equiv\text{U}$ bond even though the s - and p -orbital radius of Si is only 0.3 and 0.5 Å larger than those of C . In addition, $\text{Si}\equiv\text{U}$ triple bond is 0.34 Å longer than the sum of the triple-bond covalent radii of Pyykkö, et al.⁷¹ On the other hand, the C–U σ -bond is 82% $\text{C}(s^{1.03}p)$ + 18% $\text{U}(d^{0.96}f)$ in $\text{HC}\equiv\text{UF}_3$ and the Si–U σ -bond is 80% $\text{Si}(s^{0.06}p)$ + 20% $\text{U}(d^{0.83}f)$ in quintet $\text{Si}(\mu\text{-H})\text{UF}_3$, indicating that Si is nearly nonhybridized for σ -bonding, as shown in Table S2.²⁹ We noted before that the prerequisite for forming a $\text{C}\equiv\text{U}$ triple bond is to have highly electronegative ligands on the uranium center to stabilize the U(VI) oxidation state.²⁹ The low electronegativity of Si or the low oxidizing ability of the HSi group makes it hard to oxidize U to the $+V$ or $+VI$ oxidation states required for double or triple Si–U bonds in the HSiUF_3 molecules. As a result, uranium remains at $+IV$ oxidation state with two localized U $5f^2$ electrons in the quintet $\text{Si}(\mu\text{-H})\text{UF}_3$ molecule, thus facilitating formation of a rare triplet silylene.

To further investigate whether the single-determinant DFT and CCSD(T) calculations are reliable enough for these unusual molecular species, we have optimized the geometries of various states of $\text{Si}(\mu\text{-H})\text{UF}_3$ using CASSCF and CASPT2 methods using a (6e,11o) active space. The Si–U bond lengths, relative energies, and electron configurations of the various states of $\text{Si}(\mu\text{-H})\text{UF}_3$ molecules calculated with CASPT2 are collected in Table 3. The CASPT2 results confirm the quintet

Table 3. Optimized Si–U Distances, Relative Energies, and Electronic Configurations for Various States of $\text{Si}(\mu\text{-X})\text{UF}_3$ Molecules Calculated Using CASPT2 Method with CASSCF(6e,11o) and Basis-II

	Si–U (Å)	config. ^a	state	ΔE (kcal/mol)
X = H	2.96	$\sigma_s^2\sigma_{ }^0\pi_1^2f^2$	$^3\text{A}''$	9.44
	2.93	$\sigma_s^2\sigma_{ }^1\pi_1^1f^2$	$^1\text{A}'$	5.17
	2.90	$\sigma_s^2\sigma_{ }^1\pi_1^1f^2$	$^3\text{A}'$	1.27
X = F	2.88	$\sigma_s^2\sigma_{ }^1\pi_1^1f^2$	$^5\text{A}'$	0.00
	3.04	$\sigma_s^2\sigma_{ }^1\pi_1^1f^2$	$^3\text{A}''$	1.92
	3.02	$\sigma_s^2\sigma_{ }^1\pi_1^1f^2$	$^1\text{A}'$	3.58
	3.05	$\sigma_s^2\sigma_{ }^1\pi_1^1f^2$	$^5\text{A}'$	2.61
	3.02	$\sigma_s^2\sigma_{ }^1\pi_1^1f^2$	$^5\text{A}''$	0.00

^aOnly main configurations are listed here. The multireference characters are listed in Figures S2–S6.

ground state, which has two unpaired 5f electrons localized on U, one σ_{\parallel} -bonding electron, one π_{\perp} -bonding electron in addition to a doubly occupied low-lying orbital localized mainly on Si, consistent with the DFT optimized quintet ground state (cf. Figure 7). Here the π_{\perp} denotes the approximately π -type orbital that is perpendicular to the molecular plane containing Si(μ -X)U atoms, whereas σ_{\parallel} represents the approximately σ -type orbital along the Si–U axis. The triplet states of the $\sigma_{\parallel}^2 f^2$ configuration with U(IV) oxidation state are higher in energy than the quintet state of $\sigma_{\parallel}^1 \pi_{\perp}^1 f^2$ configuration, as revealed by the DFT and CCSD(T) results (Table 1). All these DFT and WFT calculations show that Si(μ -H)UF₃ has a Si–U single bond and quintet ground state with a U(IV) oxidation state.

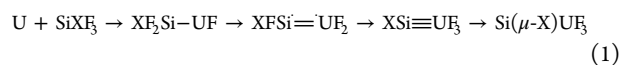
It is interesting that the lowest-energy quintet Si(μ -H)UF₃ has two one-electron σ - and π -bonding orbitals of Si–U and two electrons on the nonbonding U 5f orbitals. In order to elucidate this diradical character and the single Si–U bonding in Si(μ -H)UF₃, we also applied natural bond orbital (NBO) analysis. The compositions of the natural localized MOs (NLMOs), the Wiberg bond orders, and natural charges are listed in Table S2. It is found that Si has a 3s lone pair, a Si–H σ -bond, and two one-electron σ - and π -bonds of Si–U that are mainly composed of Si 3p orbitals, which makes Si(μ -H) similar to a monoanion, consistent with the U(IV) oxidation state. The calculated spin density is 1.37 on Si, confirming the triplet feature of the silylene group (Figure 8). Different from the common triplet state of carbene,⁷² triplet silylene is rather uncommon. Our calculations on the anion SiH[−] show that the triplet state in this bare anion is indeed more stable than the singlet state by 19 kcal/mol at B3LYP/6-311++G** level of theory. This species is reminiscent to the transition metal–ligand triplet silylene founded recently.⁷³ The UF₃ has affected the SiH fragment by stabilizing the triplet silylene. Therefore the quintet Si(μ -H)UF₃ complex with two unpaired electrons on Si can potentially be an interesting intermediate for synthetic chemistry.

The products of the U+SiF₄ system are similar to the U+SiHF₃ counterpart. As shown in Table 1, the DFT and CCSD(T) results confirm that the ground state is also quintet with a bridged Si(μ -F)UF₃ structure. While bridged silicon hydride species are well-known,^{74,75} bridged silicon–fluorine species are extremely rare. This result is not fully unexpected as driven by thermodynamics F atom strongly tends to bind with U, thus forcing Si to form bridged geometry. Similar CASPT2 results listed in Table 3 confirm that U in this system also has a +IV oxidation state with two nonbonding 5f electrons and one σ_{\parallel} -bonding electron and one π_{\perp} -bonding electron mainly from Si 3p orbital (Table 3). The other states with the same configuration $\sigma_s^2 \sigma_{\parallel}^1 \pi_{\perp}^1 f^2$ lie higher energetically than the quintet, while the states with the $\sigma_s^2 \sigma_{\parallel}^2 f^2$ configuration are much higher in energy based on both DFT and *ab initio* results (Tables 1 and 3). Note in Table 1 the D_T triplet state of the $\sigma_s^2 \sigma_{\parallel}^2 \pi_{\perp}^1 f^1$ configuration with U(V) oxidation state is calculated to be lower than the quintet state by 2.76 kcal/mol based on the PBE energies. However, the more accurate CCSD(T) calculations confirm that the D_T triplet state is about 4.86 kcal/mol higher than the quintet state with $\sigma_s^2 \sigma_{\parallel}^1 \pi_{\perp}^1 f^2$ configuration (Table 1). The calculated IR frequencies and intensities of the quintet ground state are consistent with the experiments (Table 2). For the Si–F stretching mode of the quintet state, a fingerprint of bridged Si(μ -F)UF₃ has a frequency very close to that of the U–F symmetric stretching mode, which can show as one broad band. Based on the calculated frequencies in Table 2,

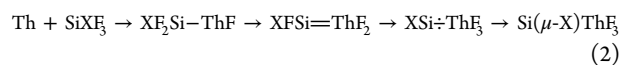
the triplet Si(μ -F)UF₃ and Si^{••}U species as well as the singlet Si≡U species have Si–F stretching bands around 501 or 831 or 836 cm^{−1}, which are not observed in the experimental spectra, indicating that the high-energy species are not formed.

In summary, the bridged Si(μ -H)UF₃ and Si(μ -F)UF₃ molecules with quintet ground states have the lowest energies among their respective isomers based on DFT and *ab initio* calculations. The agreement between the calculated IR frequencies and intensities with the experimental IR spectra thus identifies these single-bonded Si–U complexes with U(IV) oxidation state and bridged Si–X⋯U bonds. From CASPT2 geometry optimizations (Table 3), the bridged quintet Si(μ -H)UF₃ and Si(μ -F)UF₃ species have long Si–U bond lengths, ~2.88 and 3.02 Å, respectively. These distances are close to the optimized CASPT2 Si–U bond length (2.97 Å) in Cp₃U–SiPh₃.⁷⁶ They lie in the ranges of the sum of tabulated single bond radii of Si and U, 2.86 Å,⁷⁷ but are shorter than the experimentally measured Si–U bond length (3.091 Å).³⁵ Therefore the Si–U bond in the bridged species can be characterized as a reasonably strong single bond.

For the formation of the bridged reaction products, the initial step of the U+XSiF₃ reactions is presumably the laser-ablated uranium atom inserting into the XSiF₃ molecule to form XF₂SiUF (cf. Scheme 1), which can be followed by an α -F transfer to give the triplet silylidene XFSiUF₂ and then another α -F transfer to produce the likely XSiUF₃ species. Different from the analogous products from the U+XCF₃ reactions, the HSi^{••}UF₃ and XSi≡UF₃ species are metastable, and they, if exist, can easily relax to the more stable isomer with the bridged Si(μ -X)UF₃ structure. Here the nonintuitive rotation of the X–Si bond toward U is somewhat surprising based on the valence shell electron pair repulsion theory⁷⁸ and comparing the analogous C_{3v} XC≡UF₃ species.²⁹ However, because of the large difference in orbital radius Si 3s and 3p orbitals can hardly form effective sp^x hybrid orbitals; in fact in the bridged structure, Si has one lone pair of 3s electrons localized on Si and three nonhybridized 3p orbitals interacting with the X and UF₃ as revealed by the NBO analysis (Table S2). Consequently, it is natural to have the \angle X–Si–U angle as an acute angle,⁷⁹ and the rotation of the X–Si bond forms a weak Si–X⋯U interaction at little price of changing the hybridization of the Si 3s–3p orbitals. This Si–X⋯U interaction is referred to as a quasi-agostic interaction in this paper following the agostic definition from the C–H⋯M interaction.⁸⁰ The proposed reaction mechanism is illustrated in Scheme 1, which corresponds to the following series of chemical transformations:



Identifying the Reaction Products of Th+SiXF₃ Systems. In like fashion, infrared spectra for the Th and SiXF₃ reaction products are similar to those for the CXF₃ product. When comparing with the Th + CF₄ product,⁴³ the higher and lower frequency bands of the Th + SiF₄ product are blue-shifted by 5.9 and 8.8 cm^{−1}, respectively, although the CF₄ product bands are sharper. We postulate the reaction mechanism to be similar to that of the reaction of U with SiXF₃, as shown in eq 2.



Considering the similarity of the IR spectra between the products of Th + SiXF₃ and Th + CXF₃ systems, the final products of eq 2 should have the structures with three fluorine ligands on Th. Tables 4 and 5 list the optimized geometries and

Table 4. Relative DFT and CCSD(T) Energies for SiThXF₃ (X = H, F) Isomers Calculated at Optimized PBE Geometries^{a,b}

isomer	X = H		X = F	
	ΔE_{PBE}	$\Delta E_{\text{CCSD(T)}}$	ΔE_{PBE}	$\Delta E_{\text{CCSD(T)}}$
A _S XSi–ThF ₃ (C _{3v})	17.18	23.44	21.11	35.25
A _T XSi–ThF ₃ (C _{3v}) ^c	0.52	2.40	6.15	16.50
A _T ' XSi–ThF ₃ (C _s) ^c	0.58	2.41	5.16	15.97
B _S Si(μ-X)–ThF ₃ (C _s)	9.38	8.75	5.31	5.64
B _T Si(μ-X)–ThF ₃ (C _s)	0.00	0.00	0.00	0.00

^aAll the energies (in kcal/mol) are relative to those of the triplet Si(μ-X)ThF₃ isomer. ^bA_S and A_T denote, respectively, the singlet and triplet state of XSi–ThF₃ (isomer A); B_S and B_T the singlet and triplet state of Si(μ-X)–ThF₃ (isomer B). ^cThe C_{3v} symmetry constrained XSi–ThF₃ has imaginary frequencies (E₁ mode) 86i (X = H) and 48i cm⁻¹ (X = F), respectively, which can be eliminated by relaxing to the nonbridged C_s symmetry.

calculated vibrational frequencies of the singlet and triplet states of the C_{3v} XSiThF₃ and the bridged C_s Si(μ-X)ThF₃ structures using the PBE DFT method and the single-point energies calculated using CCSD(T) method at the PBE geometries. It turns out that the C_{3v} structure of triplet XSi÷ThF₃ has one imaginary frequency at the DFT level, which is stabilized by distorting to the C_s structure with an angle of ∠X–Si–Th around 157° for HSiThF₃ and 125° for FSiThF₃.

For the product of the Th + SiHF₃ reaction, the triplet states of HSi÷ThF₃ and Si(μ-H)ThF₃ structures cannot be differentiated at the PBE level. More accurate CCSD(T) calculations show that the bridged Si(μ-H)ThF₃ structure is 2.4 kcal/mol below the HSi÷ThF₃ structure. Unfortunately, the frequencies of the Si–H and Si–Th stretching modes are not observed experimentally. The PBE frequencies of the bridged isomer Si(μ-H)ThF₃ are calculated to be slightly lower than the

observed spectra. In particular, the PBE Th–F symmetric stretching frequencies are 7–10 cm⁻¹ lower than the observed neon matrix values, and no bridged Si–H modes were observed in the 1600–1700 and 700–800 cm⁻¹ regions, which are complicated by water impurity absorption and the possibility of band broadening for this mode by matrix interactions. Thus, we assign the observed spectra to Si(μ-H)ThF₃ as it has lower energy based on all the DFT, CCSD(T), and CASPT2 calculations. The calculated Th–F stretching modes of Si(μ-H)ThF₃ indeed fall around the observed neon and argon matrix values. Especially the calculated splitting pattern of vibrational frequencies (530, 528 cm⁻¹) of the Th–F asymmetric stretching mode and their intensities are in excellent agreement with the experiments (529.6, 527.6 cm⁻¹), thus supporting our identification of this molecule. The observed Th–F stretching frequencies for the Th + SiHF₃ system are 5.5 and 0.7 cm⁻¹ lower than those for the recently observed isoelectronic P÷ThF₃ pnictinidene molecule in an argon matrix.⁸¹

For the product of the Th + SiF₄ reaction, the triplet state Si(μ-F)ThF₃ species is clearly the most stable isomer similar to the uranium system above. As shown in Table 4, the singlet states of both C_{3v} FSi÷ThF₃ and C_s Si(μ-F)ThF₃ are higher than the two triplet states at DFT and CCSD(T) levels. The triplet state of C_s FSi÷ThF₃ is 5.16 kcal/mol (PBE) or 15.97 kcal/mol (CCSD(T)) higher than the triplet bridged structure, and has a Si–F stretching mode at 791 cm⁻¹, which was not observed in experiment. Therefore, both theoretical and experimental results preclude existence of FSi÷ThF₃ complex. The strongest and diagnostic Th–F stretching modes calculated for the triplet Si(μ-F)ThF₃ species are 575, 534, and 533 cm⁻¹, where the last two modes correspond to the slightly split antisymmetric Th–F stretching modes (Table 5), which fall within the observed bandwidth. The argon matrix absorptions are 10.1, 9.9, and 3.5 cm⁻¹ lower than the neon matrix bands. The Si–F stretching mode calculated at 489 cm⁻¹ for Si(μ-F)ThF₃ molecule was observed in the Ne and Ar matrix-isolation experiments, thus providing unequivocal evidence for the bridging fluorine ligand. Note that the argon–neon matrix shift for this Si–F mode is small (4

Table 5. Observed and Calculated Vibrational Frequencies for Triplet XSi÷ThF₃ and Si(μ-X)ThF₃ (X = H, F) Molecules^a

mode	obs. ^b	calcd			
		ThSiHF ₃			
		HSi÷ThF ₃ (¹ A ₁)	HSi÷ThF ₃ (³ A'')	Si(μ-H)ThF ₃ (¹ A')	Si(μ-H)ThF ₃ (³ A'')
Si–H str		2070(39)	2068(48)	1823(190)	1668(306), 748(28)
Th–F sy.	574.6 (Ne)	569(145)	571(145)	568(44)	564(153)
Str	563.6(Ar)				
Th–F as.	538.5 , 536.5(Ne)	534(337)	534(329)	530(199), 528(164)	531(171), 529(159)
Str	529.6, 527.6(Ar)				
Si–Th str			269(38)		219(25)
		ThSiF ₄			
		FSi÷ThF ₃ (¹ A ₁)	FSi÷ThF ₃ (³ A'')	Si(μ-F)ThF ₃ (¹ A')	Si(μ-F)ThF ₃ (³ A'')
Si–F str	479.4 (Ne)	836(85)	791(127)	590(86)	489(33)
Th–F sy.	579.5 (Ne)	578(174)	571(128)	567(90)	575(144)
Str	569.3(Ar)				
Th–F as.	540.4 (Ne)	537(315)	536(177), 534(155)	528(211), 521(115)	534(174), 533(198)
Str	530.5(Ar)				
Si–Th str		217(33)	190(18)	257(5)	237(39)

^aThe vibrational frequencies (cm⁻¹) and intensities (km/mol, in parentheses) are calculated using DFT PBE/TZ2P with ZORA Hamiltonian.

^bAbsorptions observed in neon (in bold face) and argon matrices.

cm^{-1}), whereas the shift for the polar Th–F bond stretching modes is large (10 cm^{-1}), consistent with common matrix effects.⁶⁶ The good agreement between the experimental and theoretical IR frequencies and intensities substantiates our identification of the triplet $\text{Si}(\mu\text{-F})\text{ThF}_3$ molecule (Table 5). For three other states, singlet FSiThF_3 (C_{3v}), triplet FSiThF_3 (C_{3v}), and singlet bridged $\text{Si}(\mu\text{-F})\text{ThF}_3$ (C_s), the calculated Si–F stretching modes are much higher than the observed modes, due to the relatively strong Si–F bond in these three species.

We also performed multireference WFT calculations by using CASPT2 method and the results are listed in Table 6.

Table 6. Optimized Si–Th Distances, Relative Energies, and Electronic Configurations for Various States of XSiThF_3 and $\text{Si}(\mu\text{-X})\text{ThF}_3$ Isomers Calculated Using CASPT2 Method with CASSCF(4e,11o) and Basis-II

isomer	Si–Th (Å)	config. ^a	state	$\Delta E(\text{kcal/mol})$
HSiThF_3	2.90	$\sigma^2\pi^2$	$^1A''$	20.00
HSiThF_3	2.90	$\sigma^2\pi^2$	$^3A''$	3.15
$\text{Si}(\mu\text{-H})\text{ThF}_3$	3.01	$\sigma_s^2\sigma_{ }^1\pi_{\perp}^1$	$^1A''$	17.82
$\text{Si}(\mu\text{-H})\text{ThF}_3$	2.99	$\sigma_s^2\sigma_{ }^1\pi_{\perp}^1$	$^3A''$	0.00
FSiThF_3	2.86	$\sigma^2\pi^2$	$^1A''$	33.52
FSiThF_3	2.85	$\sigma^2\pi^2$	$^3A''$	18.40
$\text{Si}(\mu\text{-F})\text{ThF}_3$	3.17	$\sigma_s^2\sigma_{ }^1\pi_{\perp}^1$	$^1A''$	18.98
$\text{Si}(\mu\text{-F})\text{ThF}_3$	3.15	$\sigma_s^2\sigma_{ }^1\pi_{\perp}^1$	$^3A''$	0.00

^aThe multireference characters are listed in Figures S6–S13.

The optimized bond lengths are 2.90 and 2.85 Å for triplet $\text{HSi}\ddot{\text{Th}}\text{F}_3$ and triplet $\text{FSi}\ddot{\text{Th}}\text{F}_3$, respectively, indicating partial multiple bonding in these high-energy isomers. The CASPT2 optimized bonds length are 2.99 and 3.15 Å for bridged triplet $\text{Si}(\mu\text{-H})\text{ThF}_3$ and $\text{Si}(\mu\text{-F})\text{ThF}_3$, respectively, which are slightly longer than the sum of tabulated single bond radii, 2.91 Å, for Si and Th.⁷⁷ This result suggests that the Si–Th bonds in the bridged structures are single bonds with little contribution from the unpaired electrons located primarily on nearby Si atom.

Similar to the $\text{Si}(\mu\text{-X})\text{UF}_3$ species, the $\text{Si}(\mu\text{-X})\text{ThF}_3$ species also have “triplet” silylene group as confirmed by the spin density (Figure 8). As carbon and silicon are congeners in the Periodic Table, it is interesting to compare carbenes ($:\text{CR}_2$) with silylenes ($:\text{SiR}_2$). The former usually exist in either the triplet or singlet state depending upon the nature of the substituents, while silylenes normally exist as a singlet ground state due to the large Si 3s–3p energy gap and the associated singlet–triplet gaps of around 18–21 kcal/mol.⁸² While there is continuous theoretical interest in searching of tuning ligands for ground-state triplet silylenes,⁸³ triplet silylenes are only found recently by experimentalists.⁸⁴ The present results of quintet and triplet Si–An species provide important insight in stabilizing the triplet silylenes with quasi-agostic interactions⁸⁰ between the substituent (e.g., H, F, etc.) on Si and the adjacent highly electropositive metal atom.

CONCLUSIONS

We have investigated the reaction products of laser-ablated uranium and thorium atoms with SiHF_3 and SiF_4 to explore whether early actinides such as Th and U can form multiple bonded complexes with silicon. By comparing the computed energies and vibrational spectra of XSiAnF_3 , $\text{Si}(\mu\text{-X})\text{AnF}_3$ and other isomers, we have identified the bridged $\text{Si}(\mu\text{-X})\text{AnF}_3$ (An = Th, U; X = H, F) structures as the most stable species from the matrix infrared spectra and relativistic quantum chemistry

calculations. Despite the $-\text{UF}_3$ stretching vibrations being common within 9 cm^{-1} to those from the analogous carbon species, DFT, CCSD(T), and CASPT2 calculations show that the Si–U triple-bonded singlet $\text{HSi}\equiv\text{UF}_3$ and $\text{FSi}\equiv\text{UF}_3$ with U(VI) oxidation state are higher than the double-bonded triplet $\text{HSi}^{\bullet}=\bullet\text{UF}_3$ and $\text{FSi}^{\bullet}=\bullet\text{UF}_3$ species with U(V) oxidation state and much higher than the single-bonded quintet $\text{Si}(\mu\text{-H})\text{UF}_3$ and $\text{Si}(\mu\text{-F})\text{UF}_3$ molecules with multiradical feature and U(IV) oxidation state. Furthermore, the IR spectra of the U + DSiF_3 reaction product confirmed this bridge structure of $\text{Si}(\mu\text{-D})\text{UF}_3$. Parallel investigations on thorium reactions with HSiF_3 and SiF_4 show that Th forms triplet ground states with bridged $\text{Si}(\mu\text{-X})\text{ThF}_3$ species. The calculated vibrational frequencies and qualitative infrared intensities of the stable isomers identified in this work agree well with experiments. These new multiradical compounds represent the first actinide–silicon systems with two one-electron Si–An bonds (roughly a single bond) and quasi-agostic bridged hydrogen or fluorine of an unusual “triplet” silylene group. These results suggest that, unlike in $\text{XC}\equiv\text{UF}_3$, the high orbital energies and nearly nonhybridized s–p orbitals of Si prevent the facile formation of multiple-bonded actinide–silicon species. Even though uranium bears two unpaired electrons while the adjacent silicon atom does not fulfill an octet valence shell, they do not form a triple-bonded structure as one might expect from Lewis electron pair model. The significant difference of silicon from carbon implies that formation of actinide multiple bonds with the heavier congeners of group 14 elements is challenging.

ASSOCIATED CONTENT

Supporting Information

Optimized geometry coordinates and total energies (Tables S1, S4, and S5), NBO analysis (Table S2), observed and calculated vibrational frequencies (Table S3), energy curves of ground and excitation states (Figure S1), multiconfiguration wave functions and natural orbital contours and occupations (Figure S2–S13), matrix infrared spectra for U and SiHF_3 in argon for the 1140–1000 cm^{-1} region (Figure S14). This material is available free of charge via the Internet at <http://pubs.acs.org>

AUTHOR INFORMATION

Corresponding Authors

junli@tsinghua.edu.cn
lsa@virginia.edu

Notes

The authors declare no competing financial interest.

ACKNOWLEDGMENTS

We are grateful to B. S. Ault (University of Cincinnati) and H. Willner (University of Wuppertal) for the samples of SiF_4 , SiHF_3 , and SiDF_3 . L.A. acknowledges DOE grant no. DE-SC0001034 and NCSA computing grant no. CHE07-0004N. J.L. is supported by NKBRF (2011CB932401) and NSFC (20933003, 11079006, 91026003) of China. The calculations were partially performed at Tsinghua National Laboratory for Information Science and Technology, Shanghai Supercomputing Center, and the Computer Network Information Center, Chinese Academy of Sciences. A portion of the research was performed using EMSL, a national scientific user facility sponsored by the Department of Energy's Office of Biological and Environmental Research and located at Pacific Northwest National Laboratory.

REFERENCES

- (1) Cotton, F. A.; Murillo, C. A.; Walton, R. A. *Multiple Bonds between Metal Atoms*; Springer: New York, 2005.
- (2) Moore, E. A.; Janes, R. *Metal-Ligand Bonding*; Royal Society of Chemistry: Cambridge, U.K., 2004.
- (3) Cummins, C. C. *Angew. Chem., Int. Ed.* **2006**, *45*, 862–870.
- (4) Mindiola, D. J. *Acc. Chem. Res.* **2006**, *39*, 813–821.
- (5) Gagliardi, L.; Roos, B. O. *Nature* **2005**, *433*, 848–851.
- (6) Hayton, T. W.; Boncella, J. M.; Scott, B. L.; Palmer, P. D.; Batista, E. R.; Hay, P. J. *Science* **2005**, *310*, 1941–1943.
- (7) Evans, W. J.; Kozimor, S. A.; Ziller, J. W. *Science* **2005**, *309*, 1835–1838.
- (8) Gagliardi, L.; Pyykkö, P. *Angew. Chem., Int. Ed.* **2004**, *43*, 1573–1576.
- (9) (a) Ephritikhine, M. *Dalton Trans.* **2006**, 2501–2516. (b) Cantat, T.; Arliguie, T.; Noel, A.; Thuery, P.; Ephritikhine, M.; Le Floch, P.; Mezaillies, N. *J. Am. Chem. Soc.* **2009**, *131*, 963.
- (10) Hayton, T. W. *Dalton Trans.* **2010**, *39*, 1145–1158.
- (11) Fox, A. R.; Cummins, C. C. *J. Am. Chem. Soc.* **2009**, *131*, 5716–5717.
- (12) Fortier, S.; Wu, G.; Hayton, T. W. *J. Am. Chem. Soc.* **2010**, *132*, 6888–6889.
- (13) Fox, A. R.; Arnold, P. L.; Cummins, C. C. *J. Am. Chem. Soc.* **2010**, *132*, 3250–3251.
- (14) Hayton, T. W. *Chem. Commun.* **2013**, *49*, 2956–2973 and references cited therein.
- (15) Fox, A. R.; Bart, S. C.; Meyer, K.; Cummins, C. C. *Nature* **2008**, *455*, 341–349.
- (16) Fox, A. R.; Cummins, C. C. *J. Am. Chem. Soc.* **2009**, *131*, 5716–5717.
- (17) Cooper, O. J.; Mills, D. P.; McMaster, J.; Moro, F.; Davies, E. S.; Lewis, W.; Blake, A. J.; Liddle, S. T. *Angew. Chem., Int. Ed.* **2011**, *2383*–2386.
- (18) (a) Brennan, J. G.; Andersen, R. A. *J. Am. Chem. Soc.* **1985**, *107*, 514–516. (b) Arney, D. S.; Burns, C. J.; Schnabel, R. C. *J. Am. Chem. Soc.* **1996**, *118*, 6780–6781.
- (19) Camp, C.; Pécaut, J.; Mazzanti, M. *J. Am. Chem. Soc.* **2013**, *135*, 12101–12111.
- (20) Thomson, R. K.; Cantat, T.; Scott, B. L.; Morris, D. E.; Batista, E. R.; Kiplinger, J. L. *Nat. Chem.* **2010**, *2*, 723–729.
- (21) King, D. M.; Tuna, F.; McInnes, E. J. L.; McMaster, J.; Lewis, W.; Blake, A. J.; Liddle, S. T. *Nat. Chem.* **2013**, *5*, 482–488.
- (22) Andrews, L.; Wang, X.; Gong, Y.; Vlaisavljevich, B.; Gagliardi, L. *Inorg. Chem.* **2013**, *52*, 9989–9993.
- (23) Wang, X.; Andrews, L.; Marsden, C. J. *Chem.—Eur. J.* **2005**, *14*, 9192–9201.
- (24) (a) Lyon, J. T.; Andrews, L.; Malmqvist, P.-Å.; Roos, B. O.; Yang, T.; Bursten, B. E. *Inorg. Chem.* **2007**, *46*, 4917–4925. (b) Roos, B. O.; Lindh, R.; Cho, H.-G.; Andrews, L. *J. Phys. Chem A* **2007**, *111*, 6420–6424 (CH₂=UH₂).
- (25) Lyon, J. T.; Andrews, L. *Inorg. Chem.* **2006**, *45*, 1847–1852 (CH₂=UHX).
- (26) Li, J.; H. S.; Hu, J. T.; Lyon, L.; Andrews. *Angew. Chem., Int. Ed.* **2007**, *47*, 9045–9049.
- (27) Lyon, J. T.; Andrews, L.; Hu, H.-S.; Li, J. *Inorg. Chem.* **2008**, *47*, 1435–1442 (CH₂=UF₂).
- (28) Lyon, J. T.; Hu, H.-S.; Andrews, L.; Li, J. *Proc. Natl. Acad. Sci. U.S.A.* **2007**, *104*, 18919–18924.
- (29) Hu, H. S.; Qiu, Y. H.; Xiong, X. G.; Schwarz, W. H. E.; Li, J. *J. Chem. Sci.* **2012**, *3*, 2786–2796.
- (30) Qiu, Y.-H.; Hu, H.-S.; Chen, G.; Li, J. *Sci. China Chem.* **2013**, DOI: 10.1007/s11426-013-5000-z.
- (31) (a) Andrews, L.; Wang, X.; Lindh, R.; Roos, B. O.; Marsden, C. J. *Angew. Chem. Intl. Ed.* **2008**, *47*, 5366–5370. (b) Andrews, L.; Wang, X. *Inorg. Chem.* **2009**, *48*, 6594–6598.
- (32) Zachariasen, W. H. *Acta Crystallogr.* **1949**, *2*, 94–99.
- (33) King, W. A.; Marks, T. J. *Inorg. Chim. Acta* **1995**, *229*, 343–354.
- (34) Diaconescu, P. L.; Odom, A. L.; Agapie, T.; Cummins, C. C. *Organometallics* **2001**, *20*, 4993–4995.
- (35) Porchia, M.; Brianese, N.; Casellato, U.; Ossola, F.; Rossetto, G.; Zanella, P.; Graziani, R. *J. Chem. Soc., Dalton Trans.* **1989**, 677–681.
- (36) West, R.; Fink, M. J.; Michl, J. *Science* **1981**, *214*, 1343–1344.
- (37) Sekiguchi, A.; Kinjo, R.; Ichinohe, M. *Science* **2004**, *305*, 1755–1757.
- (38) Wang, Y.; Xie, Y.; Wei, P.; King, R. P.; Schaefer, H. F., III; Schleyer, P. v. R.; Robinson, G. H. *Science* **2008**, *321*, 1069–1071.
- (39) Rodriguez, R.; Gau, D.; Kato, T.; Saffon-Merceron, N.; De Cózar, A.; Cossio, F. P.; Baceiredo, A. *Angew. Chem., Int. Ed.* **2011**, *50*, 10414–10416.
- (40) Lein, M.; Krapp, A.; Frenking, G. *J. Am. Chem. Soc.* **2005**, *127*, 6290–6299.
- (41) Lyon, J. T.; Andrews, L. *Inorg. Chem.* **2005**, *44*, 8610–8615 (CH₂=ThHX).
- (42) Lyon, J. T.; Andrews, L. *Eur. J. Inorg. Chem.* **2008**, *7*, 1047–1058.
- (43) Souter, P. F.; Kushto, G. P.; Andrews, L.; Neurock, M. *J. Am. Chem. Soc.* **1997**, *119*, 1682–1687 (U + H₂).
- (44) Andrews, L.; Citra, A. *Chem. Rev.* **2002**, *102*, 885–911 and references therein.
- (45) Pracna, P.; Margulies, L.; Cosleou, J.; Demaison, J.; Mkadmi, E. J.; Burger, H. *J. Mol. Spectrosc.* **2000**, *199*, 54–58.
- (46) Perdew, J. P.; Burke, K.; Ernzerhof, M. *Phys. Rev. Lett.* **1996**, *77*, 3865–3868.
- (47) ADF 2009.01; SCM, Theoretical Chemistry, Vrije Universiteit: Amsterdam, The Netherlands (<http://www.scm.com>).
- (48) te Velde, G.; Bickelhaupt, F. M.; Baerends, E. J.; Guerra, C. F.; van Gisbergen, S. J. A.; Snijders, J. G.; Ziegler, T. *J. Comput. Chem.* **2001**, *22*, 931–967.
- (49) Guerra, C. F.; Snijders, J. G.; te Velde, G.; Baerends, E. J. *Theor. Chem. Acc.* **1998**, *99*, 391–403.
- (50) van Lenthe, E.; Baerends, E. J.; Snijders, J. G. *J. Chem. Phys.* **1993**, *99*, 4597–4610.
- (51) van Lenthe, E.; Baerends, E. J. *J. Comput. Chem.* **2003**, *24*, 1142–1156.
- (52) (a) Becke, A. D. *J. Chem. Phys.* **1993**, *98*, 5648–5652. (b) Lee, C.; Yang, Y.; Parr, R. G. *Phys. Rev. B* **1988**, *37*, 785–789.
- (53) (a) Becke, A. D. *Phys. Rev. A* **1988**, *38*, 3098–3100. (b) Burke, K.; Perdew, J. P.; Wang, Y. In *Electronic Density Functional Theory: Recent Progress and New Directions*; Dobson, J. F., Vignale, G., Das, M. P., Ed.; Plenum, 1998.
- (54) Frisch, M. J.; Trucks, G. W.; Schlegel, H. B.; Scuseria, G. E.; Robb, M. A.; Cheeseman, J. R.; Montgomery, J. A., Jr.; Vreven, T.; Kudin, K. N.; Burant, J. C.; Millam, J. M.; Iyengar, S. S.; Tomasi, J.; Barone, V.; Mennucci, B.; Cossi, M.; Scalmani, G.; Rega, N.; Petersson, G. A.; Nakatsuji, H.; Hada, M.; Ehara, M.; Toyota, K.; Fukuda, R.; Hasegawa, J.; Ishida, M.; Nakajima, T.; Honda, Y.; Kitao, O.; Nakai, H.; Klene, M.; Li, X.; Knox, J. E.; Hratchian, H. P.; Cross, J. B.; Adamo, C.; Jaramillo, J.; Gomperts, R.; Stratmann, R. E.; Yazyev, O.; Austin, A. J.; Cammi, R.; Pomelli, C.; Ochterski, J. W.; Ayala, P. Y.; Morokuma, K.; Voth, G. A.; Salvador, P.; Dannenberg, J. J.; Zakrzewski, V. G.; Dapprich, S.; Daniels, A. D.; Strain, M. C.; Farkas, O.; Malick, D. K.; Rabuck, A. D.; Raghavachari, K.; Foresman, J. B.; Ortiz, J. V.; Cui, Q.; Baboul, A. G.; Clifford, S.; Cioslowski, J.; Stefanov, B. B.; Liu, G.; Liashenko, A.; Piskorz, P.; Komaromi, I.; Martin, R. L.; Fox, D. J.; Keith, T.; Al-Laham, M. A.; Peng, C. Y.; Nanayakkara, A.; Challacombe, M.; Gill, P. M. W.; Johnson, B.; Chen, W.; Wong, M. W.; Gonzalez, C.; Pople, J. A. *Gaussian 03*, revision A.1; Gaussian, Inc.: Pittsburgh, PA, 2003.
- (55) (a) Frisch, M. J.; Pople, J. A.; Binkley, J. S. *J. Chem. Phys.* **1984**, *80*, 3265–3269. (b) Raghavachari, K.; Trucks, G. W. *J. Chem. Phys.* **1989**, *91*, 1062–1065.
- (56) Küchle, W.; Dolg, M.; Stoll, H.; Preuss, H. *J. Chem. Phys.* **1994**, *100*, 7535–7542.
- (57) (a) Purvis, G. D.; Bartlett, R. J. *J. Chem. Phys.* **1982**, *76*, 1910–1918. (b) Scuseria, G. E.; Janssen, C. L.; Schaefer, H. F. *J. Chem. Phys.* **1988**, *89*, 7382–7387.
- (58) Woon, D. E.; Dunning, T. H., Jr. *J. Chem. Phys.* **1993**, *98*, 1358–1371.

- (59) Dunning, T. H., Jr. *J. Chem. Phys.* **1989**, *90*, 1007–1023.
- (60) Fuentelba, P.; Preuss, H.; Stoll, H.; Szentpaly, L. v. *Chem. Phys. Lett.* **1982**, *89*, 418–422.
- (61) (a) Roos, B. O.; Taylor, P. R.; Siegbahn, P. E. M. *Chem. Phys.* **1980**, *48*, 157–173. (b) Roos, B. O. *Int. J. Quantum Chem.* **1980**, *S14*, 175–189.
- (62) (a) Andersson, K.; Malmqvist, P.-A.; Roos, B. O.; Sadlej, A. J.; Wolinski, K. *J. Phys. Chem.* **1990**, *94*, 5483–5488. (b) Andersson, K.; Malmqvist, P.-A.; Roos, B. O. *J. Chem. Phys.* **1992**, *96*, 1218–1226. (c) Celani, P.; Werner, H.-J. *J. Chem. Phys.* **2000**, *112*, 5546–5557.
- (63) Werner, H.-J.; Knowles, P. J.; Lindh, R.; Manby, F. R.; M. Schütz, Celani, P.; Korona, T.; Mitrushenkov, A.; Rauhut, G.; Adler, T. B.; Amos, R. D.; Bernhardsson, A.; Berning, A.; Cooper, D. L.; Deegan, M. J. O.; Dobbyn, A. J.; Eckert, F.; Goll, E.; Hampel, C.; Hetzer, G.; Hrenar, T.; Knizia, G.; C. Köppl, Liu, Y.; Lloyd, A. W.; Mata, R. A.; May, A. J.; McNicholas, S. J.; Meyer, W.; Mura, M. E.; Nicklass, A.; Palmieri, P.; K. Pflüger, Pitzer, R.; Reiher, M.; Schumann, U.; Stoll, H.; Stone, A. J.; Tarroni, R.; Thorsteinsson, T.; Wang, M.; Wolf, A. *MOLPRO*, version 2009.1, a package of ab initio programs; University College Cardiff Consultants Limited: Cardiff, U.K. (<http://www.molpro.net>).
- (64) Jacox, M. E. *J. Phys. Chem. Ref. Data* **1994**, Monograph 3; 1998, 27 (2), 115.
- (65) (a) Buchmarina, V. N.; Gerasimov, A. Yu.; Predtechenskii, Yu. B.; Shklyarik, V. G. *Opt. Spectrosc. (USSR)* **1992**, *72*, 38. (b) unpublished IR spectra of Th reaction products with F₂ in excess argon at 5 K.
- (66) Jacox, M. E. *Chem. Phys.* **1994**, *189*, 149–170.
- (67) Li, J.; Bursten, B. E.; Liang, B.; Andrews, L. *Science* **2002**, *295*, 2242–2245.
- (68) Li, J.; Bursten, B. E.; Andrews, L.; Marsden, C. J. *J. Am. Chem. Soc.* **2004**, *126*, 3424–3426.
- (69) (a) Liang, B.; Andrews, L.; Li, J.; Bursten, B. E. *J. Am. Chem. Soc.* **2002**, *124*, 9016–9017. (b) Andrews, L.; Liang, B.; Li, J.; Bursten, B. E. *J. Am. Chem. Soc.* **2003**, *125*, 3126–3139.
- (70) (a) Andrews, L.; Liang, B.; Li, J.; Bursten, B. E. *Angew. Chem., Int. Ed.* **2000**, *39*, 4565–4567. (b) Wang, X.; Andrews, L.; Li, J.; Bursten, B. E. *Angew. Chem., Int. Ed.* **2004**, *43*, 2554–2557.
- (71) Pyykkö, P.; Riedel, S.; Patzchke, M. *Chem.—Eur. J.* **2005**, *11*, 3511–3522.
- (72) Jiang, P.; Gaspar, P. P. *J. Am. Chem. Soc.* **2001**, *123*, 8622–8623.
- (73) Sekiguchi, A.; Tanaka, T.; Ichinohe, M.; Akiyama, K.; Gaspar, P. P. *J. Am. Chem. Soc.* **2008**, *130*, 426–427.
- (74) Cordonnier, M.; Bogey, M.; Demuynck, C.; Destombes, J. L. *J. Chem. Phys.* **1992**, *97*, 7984–7989 and references therein.
- (75) Grev, R. S.; Schaefer, H. F. *J. Chem. Phys.* **1992**, *97*, 7990–7998 and references therein.
- (76) Vlasisavljevich, B.; Mir, P.; Cramer, C. J.; Gagliardi, L.; Infante, I.; Liddle, S. T. *Chem.—Eur. J.* **2011**, *17*, 8424–8433.
- (77) (a) Pyykkö, P.; Atsumi, M. *Chem.—Eur. J.* **2009**, *15*, 12770–12779. (b) Pyykkö, P.; Atsumi, M. *Chem.—Eur. J.* **2009**, *15*, 186–197.
- (78) Gillespie, R. J.; Nyholm, R. S. *Quart. Rev.* **1957**, *11*, 339–380.
- (79) Frenking, G. *Angew. Chem., Int. Ed.* **2003**, *42*, 143–147.
- (80) Brookhart, M.; Green, M. L. H.; Parkin, G. *Proc. Natl. Acad. Sci. U.S.A.* **2007**, *104*, 6908–6914.
- (81) Wang, X.; Andrews, L. *Dalton Trans.* **2009**, 9260–9265 (Th + EF₃).
- (82) (a) Balasubramanian, K.; Mclean, A. D. *J. Chem. Phys.* **1986**, *85*, 5117–5119. (b) Bauschlicher, C. W.; Taylor, P. R. *J. Chem. Phys.* **1987**, *86*, 1420–1424. (c) Trinquier, G. *J. Am. Chem. Soc.* **1990**, *112*, 2130–2137. (d) Denk, M.; Green, J. C.; Metzler, N.; Wagner, M. *J. Chem. Soc., Dalton Trans.* **1994**, 2405–2410.
- (83) (a) Grev, R. S.; Schaefer, H. F., III; Gaspar, P. P. *J. Am. Chem. Soc.* **1991**, *113*, 5638–5634. (b) Momeni, M. R.; Shakib, F. A. *Organometallics* **2011**, *30*, 5027–5032.
- (84) (a) Jiang, P.; Gaspar, P. P. *J. Am. Chem. Soc.* **2001**, *123*, 8622–8623. (b) Sekiguchi, A.; Tanaka, T.; Ichinohe, M.; Akiyama, K.; Tero-Kubota, S. *J. Am. Chem. Soc.* **2003**, *125*, 4962–4963.